

# MODEL FOR RELAXATION OSCILLATIONS OF LUMINOUS ACCRETION DISK IN GRS 1915+105: VARIABLE INNER EDGE

KEN-YA WATARAI<sup>1,2,3</sup>, SHIN MINESHIGE<sup>1</sup>

<sup>1</sup> Yukawa Institute for Theoretical Physics, Kyoto University, Sakyo-ku, Kyoto 606-8502

<sup>2</sup> Department of Astronomy, Graduate School of Science, Kyoto University, Sakyo-ku, Kyoto 606-8502

<sup>3</sup> Research Fellow of the Japan Society for the Promotion of Science

watarai@yukawa.kyoto-u.ac.jp, watarai@kusastro.kyoto-u.ac.jp

2003/6/16 draft accepted version!

## ABSTRACT

To understand the bursting behavior of the microquasar GRS 1915+105, we calculate time evolution of a luminous, optically thick accretion disk around a stellar mass black hole undergoing limit-cycle oscillations between the high- and low- luminosity states. We, especially, carefully solve the behavior of the innermost part of the disk, since it produces significant number of photons during the burst, and fit the theoretical spectra with the multi-color disk model. The fitting parameters are  $T_{\text{in}}$  (the maximum disk temperature) and  $R_{\text{in}}$  (the innermost radius of the disk). We find an abrupt, transient increase in  $T_{\text{in}}$  and a temporary decrease in  $R_{\text{in}}$  during a burst, which are actually observed in GRS 1915+105. The precise behavior is subject to the viscosity prescription. We prescribe the radial-azimuthal component of viscosity stress tensor to be  $T_{r\varphi} = -\alpha\Pi(p_{\text{gas}}/p)^\mu$ , with  $\Pi$  being the height integrated pressure,  $\alpha$  and  $\mu$  being the parameter, and  $p$  and  $p_{\text{gas}}$  being the total pressure and gas pressure on the equatorial plane, respectively. Model with  $\mu = 0.1$  can produce the overall time changes of  $T_{\text{in}}$  and  $R_{\text{in}}$ , but cannot give an excellent fit to the observed amplitudes. Model with  $\mu = 0.2$ , on the other hand, gives the right amplitudes, but the changes of  $T_{\text{in}}$  and  $R_{\text{in}}$  are smaller. Although precise matching is left as future work, we may conclude that the basic properties of the bursts of GRS 1915+105 can be explained by our “limit-cycle oscillation” model. It is then required that the spectral hardening factor at high luminosities should be about 3 at around the Eddington luminosity instead of less than 2 as is usually assumed.

*Subject headings:* accretion: accretion disks, black holes—stars: X-rays

## 1. INTRODUCTION

Microquasars in our Galaxy are enigmatic objects on account of their curious time variability, extremely large brightness (Belloni et al. 1997a, 1997b; Mirabel et al. 1994; Rao, Yadav, & Paul 2000), and energetic super-luminal jets (Mirabel & Rodriguez 1998). Large numbers of broad-band observations have been so far performed, revealing that they are low mass X-ray binaries including black holes and that the accretion flow around the black hole illuminates via the release of the gravitational energy. Their long-term bursts ( $\sim$  months) could be triggered by a thermal instability in the disk (e.g. Mineshige & Wheeler 1989), however, the mechanism causing their short-term peculiar behavior is not well understood yet (Mirabel & Rodriguez 1999; Belloni et al. 2000; Naik et al. 2002). From the theoretical viewpoints, it is interesting to investigate how their time-dependent properties of accretion disks can be understood in the frame work of the disk models.

Among plenty of Galactic black-hole candidates, GRS 1915+105, most famous microquasar, is unique in exhibiting quasi-periodic luminosity variation (Belloni et al. 1997a, 1997b). Yamaoka, Ueda & Inoue (2001) analyzed the X-ray data of GRS 1915+105, taken by ASCA and RXTE during 1998-2000 and found that it exhibits mainly two branches in its high luminosity state: the high temperature branch (HTB),  $kT \sim 2$  keV, and the low temperature branch (LTB),  $kT \lesssim 1$  keV (see also Belloni 2002). The transition time between them is  $\sim 1$  s. Interestingly, both states can be fitted by the multi-color disk model (hereafter, MCD; Mitsuda et al. 1984), however, what is puzzling in their HTB data is too high temperature and too small inner radius ( $R_{\text{in}} \sim 20$  km) to account for within the framework of the standard disk model for black-hole candidates (BHCs). It is interesting to note, in this respect, that a similar puzzle is known in ultra-luminous compact X-ray sources (ULXs, see Makishima et al. 2000, Mizuno, Kubota & Makishima 2001). In this case, several possibilities have been discussed; rotating black-hole hypothesis (Makishima et al. 2000), moderate beaming effects (King et al. 2001), and the shift of the inner edge of the disk in super-critical accretion regimes (Watarai, Mizuno, & Mineshige 2001, hereafter WMM01).

Then, why is GRS1915+105 so unique? What parameter is peculiar to GRS 1915+105? The fact that its luminosity is very large, comparable to the Eddington luminosity, indicates that this source seems to suffer very high mass accretion flow. The accretion disk theory predicts that an accretion disk becomes secularly and thermally unstable, when the mass accretion rate is very high so that the disk is radiation pressure-dominated (Lightman & Eardley 1974; Shibazaki & Hoshi 1975; Shakura & Sunyaev 1976). What are then the observable consequences of such an unstable accretion disk?

As for the solution of accretion flow at accretion rates exceeding the critical rate ( $\dot{M}_{\text{crit}} = L_{\text{E}}/c^2$ ), Abramowicz et al. (1988) found a self-consistent, steady-state solution, which is now known as the “slim disk.” It was then suggested that a near-critical disk may undergo limit-cycle oscillations, like the case of dwarf-nova outbursts, between the gas pressure-dominated standard disk and the slim disk (Kato 1983; Abramowicz, Lasota, & Xu 1986). Honma, Matsumoto & Kato

(1991, hereafter HMK91) were the first to numerically demonstrate limit-cycle oscillations between the two different states based on the slim disk model. They show that an existence of the enough radiation pressure dominated region is essential for developing the thermal instability. Szuszkiewicz & Miller (1997, 1998) confirmed their results for wider  $\alpha$  parameter ranges. The X-ray spectral variability of these oscillations was calculated by Zampieri, Turolla, & Szuszkiewicz (2001), who discussed the spectral behavior in each state and the corresponding hardening factor. More recently, Szuszkiewicz & Miller (2001) calculated the non-linear evolution of the disk with diffusion type viscosity, which is a more physical, and could also reproduce limit-cycle oscillation as in previous papers.

In the present study, we pay special attention to the behavior of the innermost region. The steady calculation of the slim disk indicates that a super-critical accretion flow can emit substantially from the part even inside  $3r_g$ , since large amount of gas exists inside  $3r_g$  because of high mass accretion flow. Therefore, it has been anticipated to see a temporary reduction of the radius of the inner edge of the disk during a burst (Watarai et al. 2000; Mineshige et al. 2000). To examine if this is the case, we carefully calculate the time evolution of the innermost part of a super-critical flow, compare the theoretical results with observations, and discuss the possibility of obtaining a simpler proof for the existence of the super-critical accretion and thus probing the disk-instability to be a cause of the light variations of GRS 1915+105. Note that previous calculations were all performed down only to the radius of  $\sim 2.7r_g$  (as in HMK91) or  $\sim 2.5r_g$  (Szuszkiewicz & Miller 1997, 1998, 2001; Zampieri et al. 2001) so that an important fraction of the total radiation release might have been missed. In the present study, we calculate the disk structure down to  $\sim 2.2 - 2.4r_g$ , well inside the sonic radius, to see an observable feature in terms of the fitting parameters more clearly. This smaller boundary is critical to test the disk-instability scenario for GRS 1915+105.

In the next section we present the basic equations and our model assumptions. We show the results of the time-dependent calculations of the flow in section 3. The comparison with the X-ray observation of the microquasar GRS 1915+105 is discussed in section 4. The last section is devoted to conclusions.

## 2. BASIC EQUATIONS AND NUMERICAL METHODS

The methods of calculation are nearly the same as those by HMK91 (see Kato, Fukue, and Mineshige 1998 for the detailed discussion on the basic equations). The basic equations are written by using the cylindrical coordinates  $(r, \varphi, z)$ . The assumptions of our calculation are; (i) a disk is axisymmetric, (ii) pseudo-Newtonian potential (Paczynsky & Wiita 1980) is adopted; that is,  $\psi = -GM/(R - r_g)$  with  $R \equiv \sqrt{r^2 + z^2}$ , and (iii) we employ one zone approximation toward the vertical direction. Here,  $r_g$  is the Schwarzschild radius defined by  $2GM/c^2 = 3 \times 10^6 (M/10M_\odot)$  cm. We use the height integrated quantities, such as

$$\Sigma = \int_{-H}^H \rho dz = 2I_N \rho H, \quad (1)$$

and

$$\Pi = \int_{-H}^H p dz = 2I_{N+1} p H. \quad (2)$$

Here,  $\Sigma$ ,  $\Pi$ ,  $\rho$ ,  $p$ , and  $H$  are surface density, height integrated pressure, mass density, total pressure, and scale height, respectively. The coefficients,  $I_N$  and  $I_{N+1}$ , are introduced by Hōshi (1977). The density and pressure are related to each other by the polytropic relation,  $p \propto \rho^{1+1/N}$ . We assign  $N = 3$  in the entire calculations (i.e.,  $I_3 = 16/35$  and  $I_4 = 128/315$ ). The equation of state is

$$p = p_{\text{rad}} + p_{\text{gas}} = \frac{a}{3} T_c^4 + \frac{k_B}{\bar{\mu} m_H} \rho T_c, \quad (3)$$

where the first term on the right hand side represents the radiation pressure ( $a$  and  $T_c$  are the radiation constant and the temperature on the equatorial plane, respectively) and the second term represents the gas pressure ( $k_B$  is the Stefan-Boltzmann constant,  $\bar{\mu} = 0.5$  is the average molecular weight, and  $m_H$  is the hydrogen mass). We assume hydrostatic equilibrium (Hōshi 1977),

$$(2N + 3) \frac{\Pi}{\Sigma} = H^2 \Omega_K^2 \equiv H^2 \frac{GM}{r(r - r_g)^2}. \quad (4)$$

Here,  $\Omega_K$  denotes the Keplerian angular frequency under the pseudo-Newtonian potential.

Mass conservation, the radial component of the momentum conservation, and angular momentum conservation are written as follows:

$$\frac{\partial}{\partial t}(r\Sigma) + \frac{\partial}{\partial r}(r\Sigma v_r) = 0, \quad (5)$$

$$\frac{\partial}{\partial t}(r\Sigma v_r) + \frac{\partial}{\partial r}(r\Sigma v_r^2) + r \frac{\partial \Pi}{\partial r} + \Pi \frac{\partial \ln \Omega_K}{\partial \ln r} = \Sigma(l^2 - l_K^2), \quad (6)$$

and

$$\frac{\partial}{\partial t}(r^2 \Sigma v_\varphi) + \frac{\partial}{\partial r}(r^2 \Sigma v_r v_\varphi) = \frac{\partial}{\partial r}(r^2 T_{r\varphi}), \quad (7)$$

Here, the velocity is expressed by  $v_r$  and  $v_\varphi$  for the radial and azimuthal components, respectively, and the angular momentum of gas is expressed by  $l$  and  $l_K$ , which are defined by  $l \equiv r v_\varphi$  and  $l_K \equiv r^2 \Omega_K$ , respectively.

The  $r$ - $\varphi$  component of viscous stress tensor in equation (7) is prescribed as

$$T_{r\varphi} \equiv \int_{-H}^H t_{r\varphi} dz = -\alpha\beta^\mu \Pi, \quad (8)$$

where  $\mu$  is a parameter ( $0 \leq \mu \leq 1$ ) and  $\beta \equiv p_{\text{gas}}/p$  (Szuszkiewicz 1990; HMK91; Watarai & Mineshige 2001). In the limit of vanishing  $\mu$ , we recover the ordinary  $\alpha$  viscosity prescription (Shakura & Sunyaev 1973). If we take the limit of  $\mu \rightarrow 1$ , on the other hand, the viscosity depends on the gas pressure only (Sakimoto & Coroniti 1981).

Finally, the energy equation is

$$\frac{\partial}{\partial t}(r\Sigma\epsilon_{\text{tot}}) + \frac{\partial}{\partial r}[r(\Sigma\epsilon_{\text{tot}} + \Pi)v_r - rT_{r\varphi}v_\varphi] = -2rF^-, \quad (9)$$

in which advective cooling, viscous, and radiative cooling are considered. The explicit form of the total energy ( $\epsilon_{\text{tot}}$ ) is

$$\epsilon_{\text{tot}} = \left[ 3(1 - \beta) + \frac{\beta}{\gamma - 1} + \frac{1}{2} \right] \frac{\Pi}{\Sigma} + \frac{1}{2}(v_r^2 + v_\varphi^2) + \psi_0(r), \quad (10)$$

where the first term on the right-hand side is the internal energy of gas ( $\gamma$  is the adiabatic index and we set  $\gamma = 5/3$  in the present calculation), the second term represents the kinetic energy, and the last term is the potential energy on the equatorial plane,  $\psi_0(r) \equiv -GM/(r - r_g)$ . Radiative cooling flux per unit surface area of optically thick medium is given by

$$F^- = \frac{8acT_c^4}{3\tau}, \quad (11)$$

where,  $\tau$  is the optical depth:

$$\tau = \bar{\kappa}\Sigma = (\kappa_{\text{es}} + \kappa_{\text{ff}})\Sigma, \quad (12)$$

where  $\bar{\kappa}$  is average opacity,  $\kappa_{\text{es}} = 0.4$  is a opacity of the electron scattering,  $\kappa_{\text{ff}} = 0.64 \times 10^{23} \bar{\rho} \bar{T}^{-7/2}$  is the absorption opacity via thermal Bremsstrahlung, and  $\bar{\rho} = 16/35\rho$  and  $\bar{T} = 2/3T_c$  are vertically averaged density and temperature, respectively. We solve equations (5)–(7) and (9) by modified Lax-Wendroff method with artificial viscosity.

To examine the behavior of the innermost part of the accretion flow, the calculations are performed from the outer radius at  $2000r_g$  down to the inner radius  $\sim 2.2r_g$  through the transonic point (Matsumoto et al. 1984). The number of total mesh is  $400 \sim 500$  and each mesh point is distributed uniformly on the logarithmic scale at large radii,  $r > 3.2r_g$ , and also uniformly but on the linear scale at smaller radii, where each mesh size is  $\sim 0.01r_g$ . We fixed the black-hole mass to be  $m = 10$  ( $m = M/M_\odot$ , where  $M_\odot$  is solar mass) and the viscosity parameter to be  $\alpha = 0.1$ . The critical accretion rate,  $\dot{M}_{\text{crit}}$ , is defined by  $L_E/c^2$ , where  $L_E$  is the Eddington luminosity and  $c$  is the speed of light. We define the dimensionless accretion rate to be  $\dot{m} \equiv \dot{M}/\dot{M}_{\text{crit}} = \dot{M}c^2/L_E$  throughout the present study.

### 3. TIME EVOLUTION OF THE INNER DISK

#### 3.1. Bolometric Light Curves

We first show the calculated light curves for models with  $\mu = 0$  (by the solid curve), 0.1 (by dotted curve) and 0.2 (by the dashed curve) in figure 1. The bolometric luminosity is calculated by integrating  $2\pi F^-(r)$  from the inner edge at  $r = 2.2r_g$  (at  $r = 2.4r_g$  for  $\mu = 0.1$  case) to the outer edge at  $r = 2000r_g$ . Eddington luminosity for a  $10M_\odot$  black hole is  $1.25 \times 10^{39}$  ( $M/10M_\odot$ )  $\text{erg s}^{-1}$ . For simplicity, we assume blackbody radiation field (see section 3.4 for corrections).

In model with  $\mu = 0$ , the disk luminosity suddenly rises on timescale of  $\lesssim 5(M/10M_\odot)\text{s}$ , keeps a high value for  $\sim 10(M/10M_\odot)\text{s}$ , and then decays. These time scales roughly correspond to the viscous timescale,  $t_{\text{vis}} \sim \alpha^{-1}\Omega^{-1}(r/H)^2$ , in the inner region. Namely,

$$t_{\text{vis}} \sim 1.6 \left( \frac{M}{10M_\odot} \right) \left( \frac{r}{5r_g} \right)^{3/2} \left( \frac{\alpha}{0.1} \right)^{-1} \left( \frac{H/r}{0.1} \right)^{-2} \text{ sec}. \quad (13)$$

The amplitude of the burst is about one order of magnitude. Here, we calculated the same model as that in HMK91, i.e.,  $\mu = 0$ ,  $\dot{m} = 0.96$ ,  $m = 10$ , and  $\alpha = 0.1$ . We confirmed that the amplitude and the duration of the burst in our calculation agree with those of HMK91 ( $t_{\text{burst}} \sim 15$  second for this parameter set). We continued calculations until  $\sim 2000$  second (that is,  $2 \times 10^7$  ( $r_g/c$ ) calculation steps), however, we could not obtain a next burst in the same parameters as those in HMK91. In our calculation, small oscillations (or small bursts) took place near to the critical accretion rate for many times. Moreover,  $\mu = 0$  model takes a lot of recurrence time so that observational feature of GRS1915+105 does not agree with  $\mu = 0$ . Hence, we will show  $\mu = 0.1$  model instead of  $\mu = 0$  model in the next section.

In model with  $\mu = 0.2$ , in contrast, the amplitude of the burst is less, only about  $\sim 2$  mag (about a factor of  $\sim 6$  variations). The burst rise time is somewhat longer than in the previous case but not significantly. Both of the bolometric light curves look quite similar to those obtained by HMK91, who also found that the burst amplitude and time scale are sensitive to the parameter,  $\mu$ . The different burst amplitudes can be understood in terms of the different shapes of the S-shaped thermal equilibrium curves, since the ranges of surface density (and thus of effective temperature), in which solutions are unstable, shrinks with increasing  $\mu$  (HMK91). We will explain detailed evolution in the next two subsections.

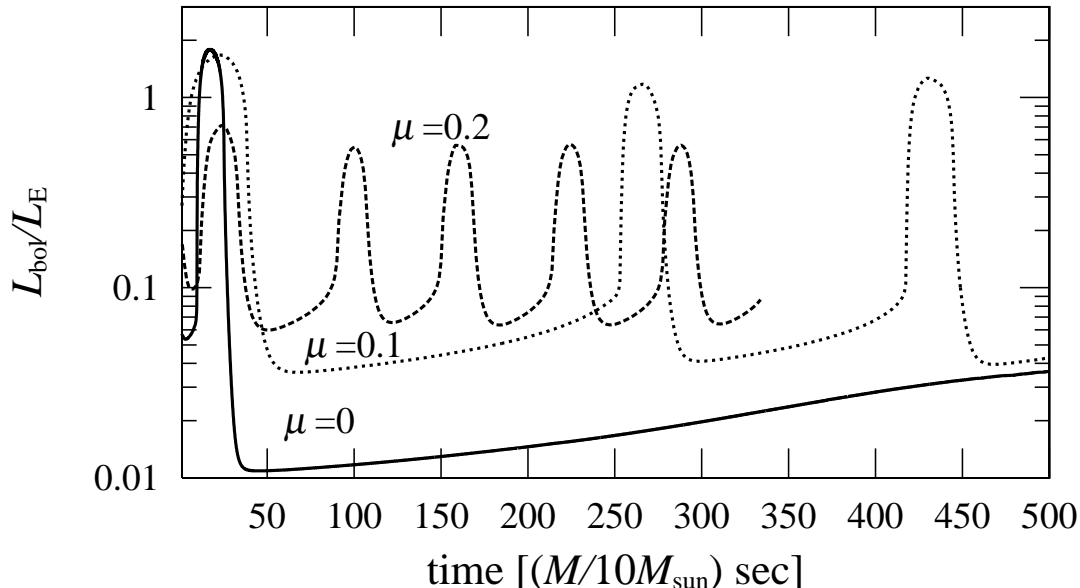


FIG. 1.— Bolometric light curves for different  $\mu$  parameters ( $\mu=0, 0.1$  and  $0.2$ ). The bolometric luminosity is defined by  $L_{\text{bol}} \equiv \int 2\pi r^2 F^- dr$ . The bolometric luminosity is normalized by the Eddington luminosity.

### 3.2. State transition: case of $\mu = 0.1$

As we mentioned in previous subsection, we can not obtain perfectly relaxed solutions in case of  $\mu = 0$  so that we will show  $\mu = 0.1$  case. We apply the data at third burst in figure 1, because the first burst is affected by initial conditions.

Figure 2 illustrates the evolution of the radial distributions of the surface density (top) and effective temperature (bottom). We set mass input rate of  $\dot{m}_{\text{in}} = 3.0$  and  $\mu = 0.1$ . The numbers in each panel indicate the order of the evolution sequence from third burst of  $\mu = 0.1$  model in figure 1.

The solid curve indicated by the number ‘1’ represents the state before the burst. In the prior burst state, radiation pressure exceeds the gas pressure from  $\sim 5r_g$  to  $20r_g$ .

Initially, there is little mass inside  $3r_g$  (this radius corresponds to the radius of the marginally stable circular orbit around a non-rotating black hole). Surface density abruptly drops by 4 orders of magnitude inside  $3r_g$  in the initial state, because the radial velocity of the gas prominently increases near the transonic point. After  $\sim 5(M/10M_{\odot})$ s, a burst starts. A thermal instability is ignited in the innermost region and an upward transition from the radiation pressure-dominated standard-disk branch to the slim-disk one is initiated there. Then, a transition wave propagates outward and the outer zone subsequently undergoes an upward transition. Once the instability sets out, the efficiency of angular momentum extraction becomes largely enhanced, thus, gas in the disk being able to fall into the black-hole rapidly. Thus, surface density in the inner part shows a rapid decline. This enhanced mass flow fills the inner empty zone, and, hence, the surface density inside  $3r_g$  suddenly increases by more than one order of magnitude.

The effective temperature distribution also shows interesting features. The most important feature seen around the peak is that because of enhanced mass flow toward the innermost part the temperature inside  $3r_g$  keeps a rather high value,  $> 10^7$  K, so that significant amount of radiation is now expected from there. This property can be seen in figure 11 of Abramowicz et al. (1988) and in figure 2 of Watarai et al. (2000) have explicitly demonstrated that this is observable. In the high, slim-disk state, the maximum temperature is slightly higher and the inner disk radius becomes smaller than in the low, standard-disk state. The radial distribution of the effective temperature in time sequence numbers 3 are proportional to  $r^{-1/2}$ , which is in good agreement with the analytical prediction (Watarai & Fukue 1999; Wang & Zhou 1999). We plotted  $r^{-1/2}$ ,  $r^{-3/4}$  slopes in figure 2b, 3b for reference.

Another notable feature is found in the subsequent evolution. When the instability wave reaches  $\sim 100r_g$ , a downward transition from the slim-disk branch to the standard-disk one begins from the inner region and again propagates outward. In both phases the transition is initiated from the inner region and the instability is propagated outward. Although these features are basically the same as those of the previous works (HMK91), we find interesting features in the behavior of the innermost region, which has been unclear in the previous calculations because of the larger truncation radius. This produces interesting observable effects. It should be noted that effective optical thickness at the inner region is more than unity during the burst phase. Hence, we can expect thermal emission around the disk inner region.

On the other hand, we have confirmed that a relatively large viscosity parameter,  $\alpha \sim 0.1$ , is required to reproduce the observations of GRS1915+105. If we adopt a smaller viscosity parameter, which tends to increase surface density and thus optical depth, the duration becomes longer than the observed value. Therefore, we conclude that  $\alpha$  is likely to be about 0.1 and some additional sources, such as metals, may contribute and raise opacities.

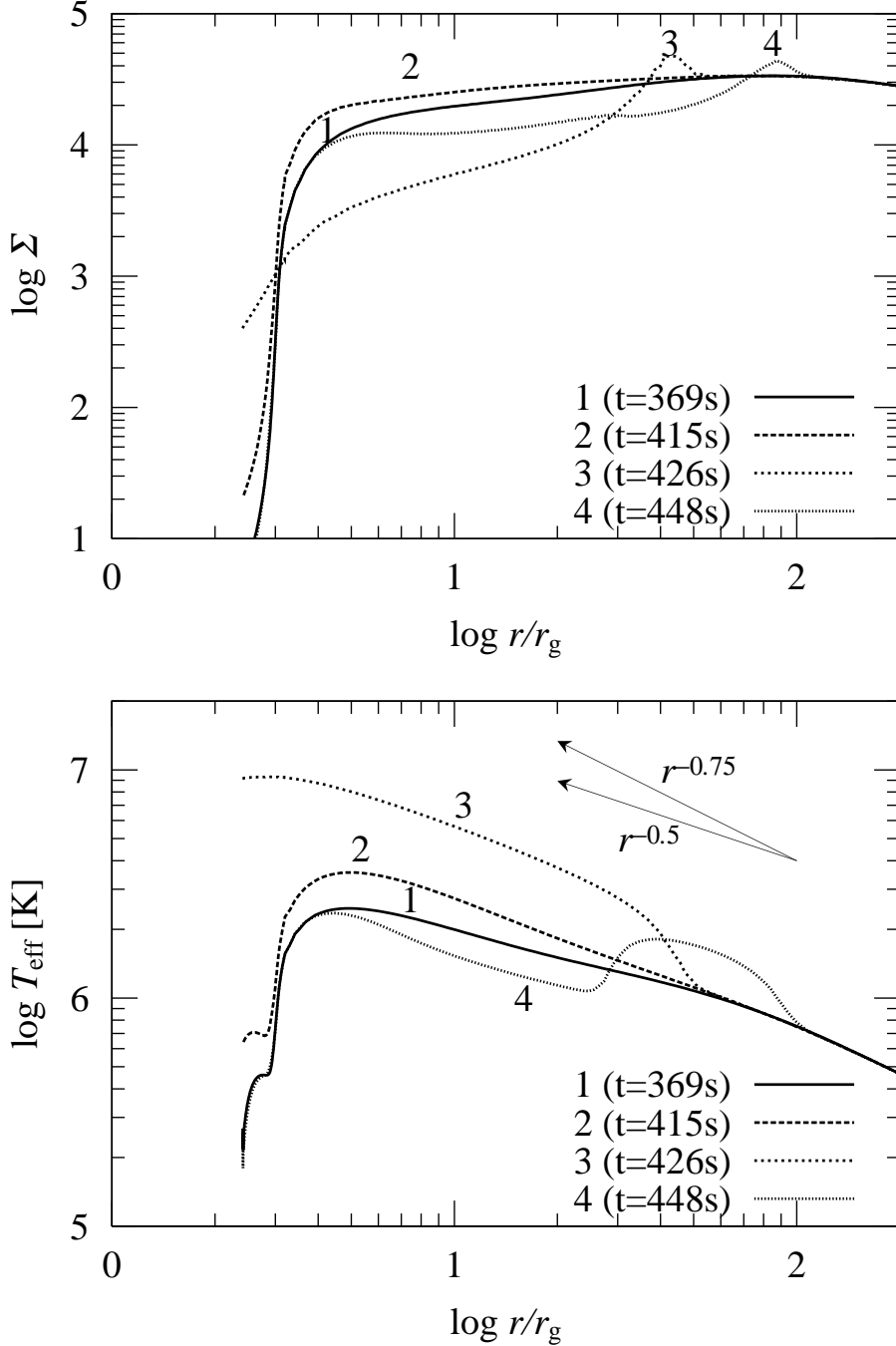


FIG. 2.— Time evolution of the surface-density profile (top) and the effective temperature profile (bottom) for the case with  $\mu = 0.1$ . The numbers 1 – 4 indicate the time sequence numbers (see figure 1). The solid curve labeled with the number 1 represents prior burst profile. The thick dashed lines (time sequence 2), dotted lines (time sequence 3), and small dashed lines represent the profiles in the rise, peak, and decay phases, respectively. Black-hole mass and the viscous parameter are  $M = 10M_{\odot}$  and  $\alpha = 0.1$ . We assume a constant mass input at a rate of  $\dot{m}_{\text{in}} = 3.0$ .

### 3.3. Different viscosity prescription: case of $\mu = 0.2$

Honma et al. (1991) used the viscosity prescriptions given by equation (8) and discussed how different prescriptions affect the overall disk evolution. They have demonstrated that in the case with  $\mu = 0.25$  the burst duration is shorter and the amplitude is smaller both by a factor of  $\sim 2$ , compared with the case with  $\mu = 0$ . That is, modifying viscosity prescription leads to drastic changes in the amplitudes of light variations and in the burst duration. We also test the case with  $\mu = 0.2$  and display the resultant light variations in figure 1 and the structural evolution in figure 3. Radiation pressure dominates over gas pressure from  $\sim 4r_g$  to  $65r_g$  in the initial state ( $\dot{m}_{\text{in}} = 3.0$ ).

Interestingly, some differences are found. Although the surface density and the temperature of the innermost region are still variable, the way of time changes are qualitatively different from the previous case. The upper panel of figure

3 indicates that the instability evolves less efficiently than in the case with  $\mu = 0$ . Especially, surface density remains very low inside  $3r_g$  even at the peak and the maximum temperature does not exceed  $10^7$  K. Moreover, the maximum temperature is reached at  $\sim 4 - 6r_g$  unlike the previous case, in which temperature is maximum at the inner edge.

The reason for this change can be understood as follows: Non-zero  $\mu$  values lead to a reduction of  $\alpha$  when the radiation pressure is larger than the gas pressure ( $p_{\text{rad}} > p_{\text{gas}}$ ). This reduction tends to increase the surface density of the equilibrium solution at a fixed mass accretion rate (since  $\alpha\Sigma \propto \dot{M}$  in the steady condition), and the amount of this increase gets larger, as  $\dot{M}$  increases. In other words, the S shape of the thermal equilibrium curves get less prominent, as  $\mu$  increases (see Kato et al. 1998, figure 10.4). As a result, the thermal instability tends to be suppressed.

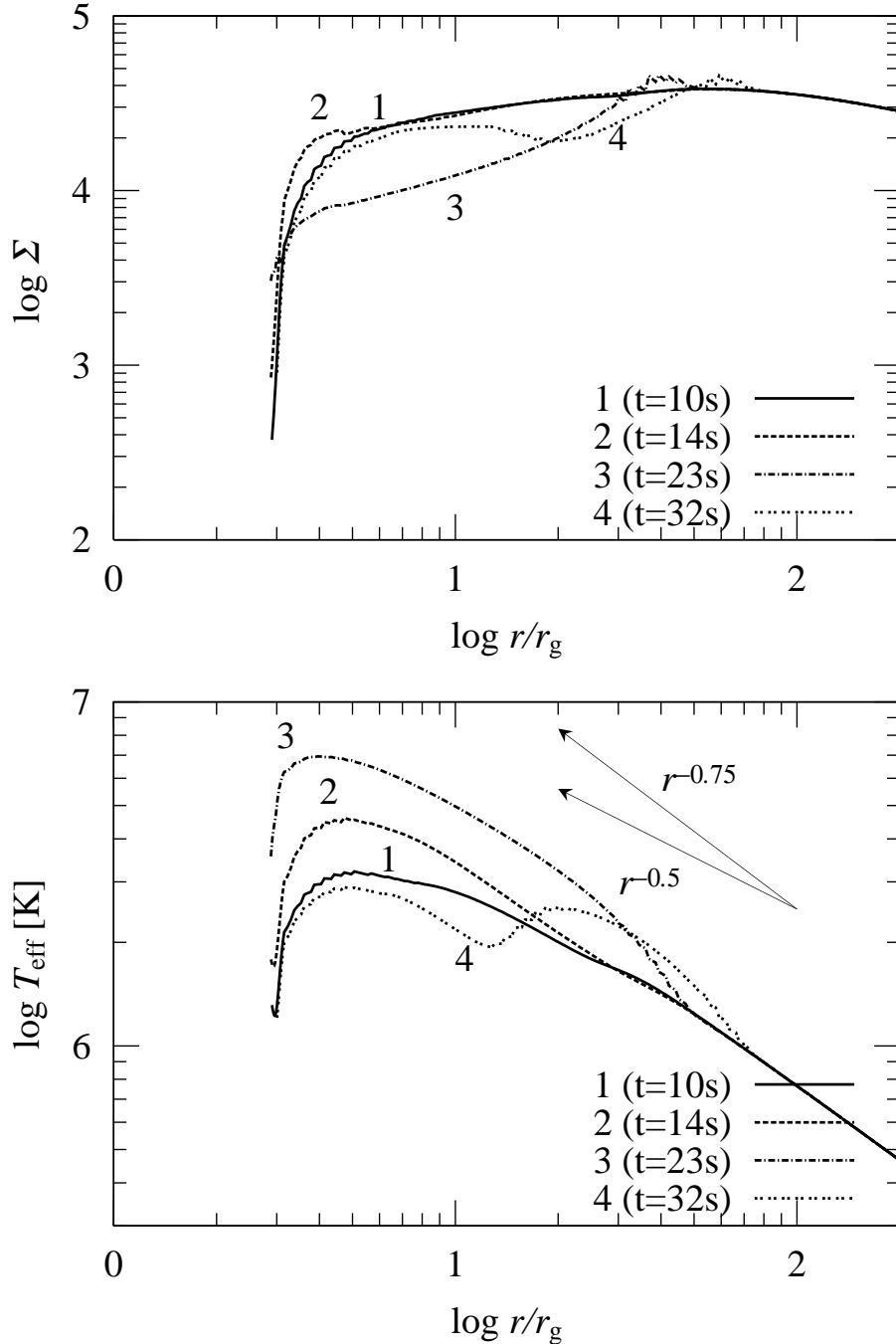


FIG. 3.— The same as figure 2 but for the case with  $\mu = 0.2$  (We prescribe the  $r$ - $\varphi$  component of the shear stress tensor to be  $T_{r\varphi} = -\alpha\Pi(p_{\text{gas}}/p)^\mu$ ). We assume a constant mass input at a rate of  $\dot{m}_{\text{in}} = 3.0$ . Other parameters are the same as those in figure 2. Note that even at the peak surface density abruptly decreases inside  $3r_g$  and the temperature maximum is reached outside  $3r_g$ , which makes a big contrast to the case with  $\mu = 0.1$ .

We next perform the spectral fitting to the calculated spectra in the same manner as that adopted by WMM01. First, we calculate the spectra based on our calculation, assuming blackbody radiation at each radius for each time step. Then, we fit the spectra with the MCD model (Mitsuda et al. 1984), from which we can derive the disk maximum temperature,  $T_{\text{in}}^0$ , and the radius,  $R_{\text{in}}^0$ , of the region emitting blackbody radiation with  $T_{\text{in}}^0$ . Before making a direct comparison with the observations we need the following corrections: (i) The derived value of  $R_{\text{in}}^0$  is influenced by the effects of the inner boundary condition as well as general relativistic effects; that is, the value tends to be overestimated, in general, compared with the real inner-edge radius. We thus need to introduce a correction factor  $\eta = 0.41$  and set  $R_{\text{in}} = \eta R_{\text{in}}^0$  (Kubota et al. 1998). (ii) Second, the disk spectra are not perfectly blackbody but are modified by the Compton scattering effects, which lead to spectral hardening (Ross, Fabian, & Mineshige 1992; Shimura & Takahara 1995). Zampieri et al. (2001) also estimated the spectral hardening factor through solving the radiation transfer in the vertical direction, and found results, which mostly agree with Shimura & Takahara (1995). The actual value is  $\kappa \approx 1.7$  for stellar mass black hole and increases with increasing  $\dot{M}$ .

Unfortunately, it is difficult to precisely predict the spectral hardening factor due mainly to the uncertainties in metal opacities (which depend on the metal ionization stages, amount of incident X-ray photons, etc). Poorly understood disk-corona structure should also modify the model spectra. Also it strongly depends on the line of sight of observation, and the radial motion of the flow. Previous works (Shimura & Takahara 1995; Wang et al. 1999; Zampieri et al. 2001) solved the radiation transfer in the vertical direction, assuming that, the photons can escape only in the vertical direction. For high accretion rate disk, however, the advected flow can trap significant fraction of photons; the photons propagate not only in the vertical direction but also in the radial direction. According to the preliminary results by Ohsuga, Mineshige, & Watarai (2003), the spectral hardening factor changes from 1.2 to about 2.3. This hardening factor depends on the disk model. Thus, the spectral hardening factor possibly exceeds 2.0. In recent study Shimura & Manmoto (2002) also show that the general relativistic effect is important for solving the radiation transfer equations including the photon trapping. According to their results the hardening factor is more than  $\kappa > 100$  in extreme Kerr hole and high mass accretion rate case ( $\dot{m}=100$ ). We have not yet reached the consensus what the most appropriate value is. Therefore, we treated the hardening factor as a parameter.

Here we adopt relatively large value  $\kappa = 2.0$  because of high  $\dot{M}$  cases being considered here and set the color temperature to be  $T_{\text{in}} = \kappa T_{\text{in}}^0$ . The effects of inclination angle and Doppler beaming are ignored in the present fitting.

Figure 4 displays the time variations of the X-ray luminosity, maximum temperature ( $T_{\text{in}}$ ), and the inner edge radius of the disk ( $R_{\text{in}}$ ), from the top to bottom, respectively (we also fitted the initial burst for  $\mu = 0$  model).

We calculated the X-ray luminosity by using  $R_{\text{in}}$  and  $T_{\text{in}}$ , following equation (4) in Makishima et al. (2000). In the rise phase the luminosity increases by about one order of magnitude,  $T_{\text{in}}$  increases by a factor of  $\sim 3$ , and  $R_{\text{in}}$  decreases by a factor of  $\sim 2$ . At the end of the decay phase (corresponding to the time sequence 4) we see a transient rise in  $R_{\text{in}}$ . This is because in this phase the temperature profile is rather flat up to  $\sim 50r_g$  so that the fitting is affected by the emission from this extended regions. However, the transient rise may depend on the energy range used for fitting.

We note that to see the significant variation of  $R_{\text{in}}$ , we should set the inner boundary of the disk as small as possible. Interestingly, however, evolutionary paths are different for the rise and decay phases in these diagrams. We will discuss about the comparison between our model and the observed objects in the next section.

## 4. DISCUSSION

### 4.1. Comparison with the observation of Microquasar GRS 1915+105

We have calculated the time evolution of a near-critical accretion disk undergoing the relaxation oscillations between the low mass accretion rate branches and high mass accretion rate branches. We, especially, focus our study on the time changes of the apparent inner-edge radius,  $R_{\text{in}}$ , and the maximum temperature,  $T_{\text{in}}$ , finding peculiar behavior during the course of one burst cycle. In this subsection we discuss to what extent our model calculation can explain the X-ray observations of GRS 1915+105.

Figure 5 shows the results of the fitting to the observational data of GRS 1915+105 made by Yamaoka et al. (2001) based on the MCD model. It is clearly seen in this figure that the temperature increases and the inner radius decreases in the burst phase (see also Taam, Chen, & Swank 1997). This is what we obtained in the calculations with  $\mu = 0.1$ , thus we can conclude that qualitative features can be explained by our model.

However, the precise fitting is not easy. According to model calculations, the burst properties can vary by changing the black-hole mass,  $\alpha$  parameter, or viscosity prescriptions. Although the observed time changes of  $T_{\text{in}}$  and  $R_{\text{in}}$  agree well when  $\mu = 0.1$ , the burst amplitude is too large to reconcile with the observation. Model with  $\mu = 0.2$ , in contrast, can reproduce the observed amplitudes of the luminosity variations during the burst, but the shape of the light curve does not match the observation in the sense that the burst rise is slower than that of the observation. The observed time changes in  $T_{\text{in}}$  and  $R_{\text{in}}$  are not reproduced, neither. That is, we cannot perfectly fit the observations by simply changing the  $\mu$  value. Likewise, changing  $\alpha$  values does not alter the results qualitatively, but just results in changing the timescales. If we take smaller  $\alpha$ , say  $\alpha = 0.01$ , we will obtain longer burst duration, about 19 s, since the burst duration time is  $\propto \alpha^{-0.64}$  (HMK91).

We should also remark that the absolute value of temperature is not well reproduced, since  $T_{\text{in}} \sim 1\text{keV}$  in the observations, whereas  $T_{\text{in}} \sim 0.6\text{keV}$  in our model, even if we adopt a large spectral hardening factor of  $\kappa \sim 2.0$ . To fit the observations during the low-luminosity state, we need to require that there should be additional mechanisms to further harden the spectral so as to achieve  $\kappa \sim 3$ . As mentioned Introduction, this issue is common to other high-luminosity

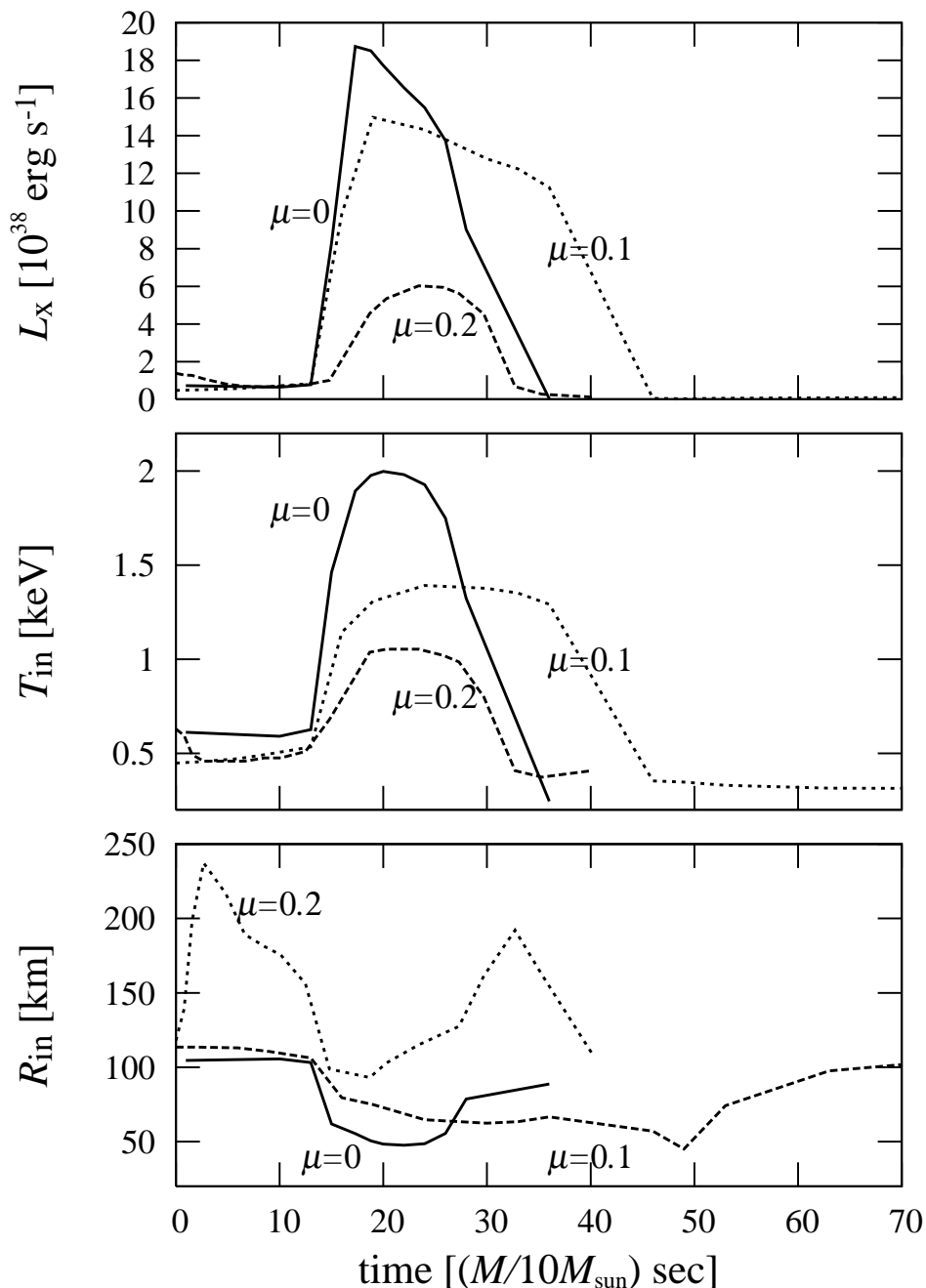


FIG. 4.— Time variations of the X-ray luminosity,  $L_X$ , the maximum temperature,  $T_{\text{in}}$ , and the inner disk radius,  $R_{\text{in}}$ , respectively. The horizontal axis is the elapsed time in sec. The solid, dashed, and dotted curves represent the cases with  $\mu = 0$ ,  $\mu = 0.1$ , and  $\mu = 0.2$ , respectively. All the spectra are fitted in the energy range of 2.0-20 keV (for burst phase) and 2.0-10 keV (for decay phase).

sources, such as ULXs.

There also exist other uncertainties arising due to jet or wind, corona, Compton scattering effects, and so on. Also, the determination of the inclination angle is very important. Recently some authors argue that dissipation of energy in disk corona or in jets can affect the disk evolution (Nayakshin et al. 2000; Janiuk, Czerny, & Siemionowska 2000). They propose the phenomenological model, in which they assume the total gas energy in both disk and jet components to be conserved and seek for the functional form, which matches the observed burst duration and luminosity. It is then found that the fraction of the jet energy has to increase during the burst phase to match the observation. However, there is no strong physical basis on this suggestion.

If some dissipation processes like corona, jet or wind work around the peak, the amplitude of the burst get smaller, which might help. In other words, we need to somehow modify the S-shaped thermal equilibrium curves by changing



$\alpha$  as a function of temperature, by including dissipation processes in jets or corona at the peak, or something else. It might be interesting to note that the disk-instability model for dwarf-nova outbursts has a similar problem; the constant  $\alpha$  model cannot produce clear-cut outburst-quiescence light curves but instead only exhibits small-amplitude fluctuations (see, e.g., figure 1 of Mineshige & Osaki 1985). To fit the observations, therefore, one needs to increase  $\alpha$  values in the hot state, compared with that in the cool state, by a factor of  $\sim 3$ .

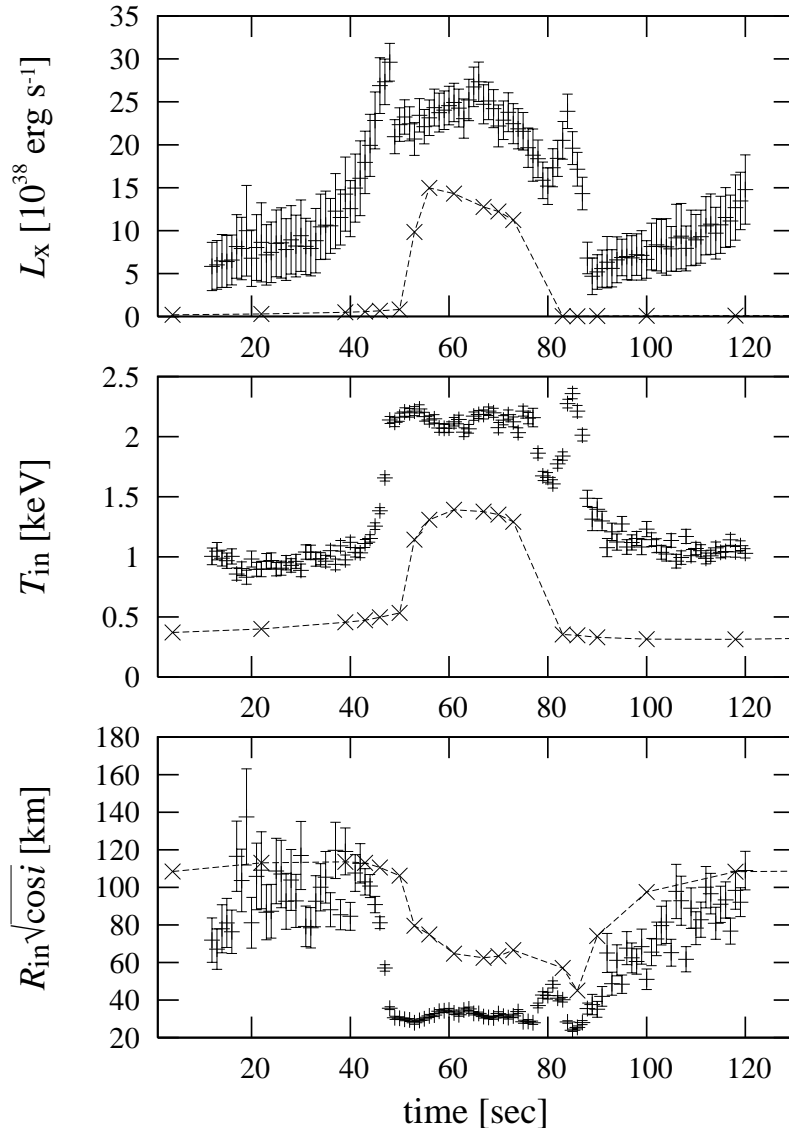


FIG. 5.— The same as figure 4 but from the observations of GRS 1915+105 (courtesy of K. Yamaoka). Cross plus dashed lines represent the derived fitting parameters on  $\alpha = 0.1, \mu = 0.1$  model. We assume the spectral hardening factor  $\kappa = 1.7$ . The inclination angle  $i$  and the distance  $D$  are assumed to be  $i = 70$  and  $D = 12.5$  kpc (Mirabel & Rodriguez 1994).

#### 4.2. Is there a Kerr black hole?

In the high mass-accretion-rate flow, the disk inner edge can be smaller than  $3r_g$  even for a non-rotating black-hole (Watarai et al. 2000). On the other hand, it is well known that the case of a Kerr black-hole can also explain the high disk temperature and small inner-disk radius, as are observed, because of smaller radius of the marginally stable orbit. If the black hole is an extreme Kerr black hole, especially, the disk inner edge should be as small as  $0.5r_g$ .

Recently, mass estimation was made for the black hole of the microquasar GRS 1915+105, which is  $14 \pm 4M_\odot$  (Greiner et al. 2001). The corresponding Schwarzschild radius is  $42 \pm 12$  km. If we take the face value derived by Yamaoka et al. (2001), the inner radius of the disk should be  $R_{\text{in}} \geq R_{\text{in}} \sqrt{\cos i} \sim 30$  km during the burst, while  $R_{\text{in}} \sim 21$  km for the extreme Kerr hole. This result seems to rule out the extreme Kerr hole interpretation at least for GRS 1915+105, however, we should keep in mind that we are only able to detect photons practically from the region outside  $\sim 2r_g$  ( $\sim$

82 km) owing to the significant photon redshifts. It thus follows that it is not easy to distinguish whether there exists an extreme Kerr black hole or not.

At present, therefore, both possibilities (the Kerr hole and the super-critical accretion) are viable, but we can at least rule out the extreme Kerr hole case, since then  $R_{\text{in}}$  should stay constant at a small value, not depending on the luminosity of the disk, contrary to the observations.

#### 4.3. Uniqueness of GRS 1915+105

The greatest mystery involved with GRS 1915+105 resides in why only this source exhibits various types of activities, including quasi-periodic light oscillations. High mass accretion rates may not be the only reason, since other luminous sources, like GS 2023+338, whose luminosities seem to reach the Eddington luminosity (Tanaka 1989) did not record similar behavior. Further, Kubota et al. (2001) analyzed the X-ray spectrum in some Galactic black hole candidates, revealing that XTE J1550–564, one of the most well-observed microquasars with RXTE, does not behave like GRS 1915+105 during the outburst, although the spectrum evolution is somewhat similar to that of GRS 1915+105; i.e.,  $T_{\text{in}}$  increases and  $R_{\text{in}}$  decreases, as the luminosity increases in their burst phase. They also indicate that the spectrum of XTE J1550–564 can be best fit if we add the anomalous (Comptonized) component in the decay phase, whereas no such component is needed in the rise phase. This means, the disk structure differs in the rise and decay phases. What discriminates these objects and other canonical black hole X-ray transients? Do other bright ultra-luminous X-ray sources show bursting properties similar to GRS 1915+105 but not observed yet? These still remain unsolved problems.

It is interesting to note in this respect that for relatively large viscous parameter,  $\alpha \gtrsim 0.3$ , a transition from the optically thick standard-disk branch to the optically thin ADAF occurs (Takeuchi & Mineshige 1998). The transition timescale is less than a few sec for a stellar mass black-hole ( $M_{\text{BH}} = 10M_{\odot}$ ). It might be that the solution is not unique and some hidden parameter triggers the different behavior of near-critical accretion flow.

### 5. CONCLUSIONS

We calculated the evolution of the inner part of the high-luminosity accretion disk, carefully considering the transonic nature of the flow in the innermost region. We obtain the following results:

1. Our calculations confirm the previous results that the state transitions between the standard-disk and slim-disk branches occur during the burst phase. Around the burst peak, the inner edge of the disk lies at  $< 3r_g$  and there are significant photons coming from the region inside  $3r_g$ .
2. To inspect the X-ray observational features in GRS1915+105, we performed spectral fitting to the calculated spectra with the fitting parameters of  $T_{\text{in}}$  and  $R_{\text{in}}$ . As to model with  $\mu = 0.1$  we find an abrupt transient increase in  $T_{\text{in}}$  and a temporary decrease in  $R_{\text{in}}$  during an outburst, both of which were actually observed in microquasar GRS 1915+105. However, the amplitudes of light variations and the absolute value of  $T_{\text{in}}$  are too large to reconcile with the observational data. When  $\mu = 0.2$ , in contrast, the burst amplitude agrees with the observed one, but the behavior of  $T_{\text{in}}$  and  $R_{\text{in}}$  differ from the observed one. It is difficult to match the observation by simply varying  $\alpha$  or  $\mu$ . It is also important to note that the fitting results are sensitive to the photon energy range used for the fitting.
3. To summarize, although the precise fitting is left as future work, we can safely conclude that our “limit-cycle oscillation” model can explain the basic observational features of GRS 1915+105. It is then required that the spectral hardening factor at high luminosities close to the Eddington luminosity should be about 3 instead of less than 2 as is usually assumed. This means, we need additional mechanism that causes a further spectral hardening.

The authors thank the Yukawa Institute for Theoretical Physics at Kyoto University. Discussions during the YITP workshop YITP-W-01-17 on “Black Holes, Gravitational Lens, and Gamma-Ray Bursts” were useful to complete this work. Especially, we would like to thank R. Narayan, C. Done, K. Yamaoka and T. Kawaguchi for useful comments and discussions. Numerical computation in this work was carried out at the Yukawa Institute Computer Facility. This work was supported in part by the Grants-in Aid of the Ministry of Education, Science, Sports, and Culture of Japan (14001680, KW).

### REFERENCES

- Abramowicz, M.A., Czerny, B., Lasota, J.P., Szuszkiewicz, E. 1988, ApJ, 332, 646
- Abramowicz, M.A., Lasota, J.P., Xu, C. 1986, in Quasars (Proc. of IAU Symp. No. 119), ed. G. Swarup & V.K. Kapahi (D. Reidel, Dordrecht), p.371
- Belloni, T., et al. 1997a ApJ, 479, L145
- Belloni, T., et al. 1997b ApJ, 488, L109
- Belloni, T., Klein-Wolt, M., Mendez, M., van der Klis, M., & van Paradijs, J. 2000, A&A, 355, 271
- Belloni, T. 2002, astro-ph/0208129
- Greiner, J., Cuby, J.G., McCaughrean, M.J. 2001, Nature, 414, 522
- Janiuk, A., Czerny, B., Siemionowska, A. 2000, ApJ, 542, L33
- Honma, F., Matsumoto, R., Kato, S. 1991, PASJ, 43, 147 (HMK91)
- Hōshi, R. 1977, Prog. Theor. Phys., 58, 1191
- Kato, S., 1993, in Theoretical Aspects in Structure, Activity, and Evolution of Galaxies, ed. S. Aoki & Y. Yoshii (Tokyo Astron. Obs., Tokyo), p.32
- Kato, S., Fukue, J., Mineshige, S. 1998, Black-Hole Accretion Disks (Kyoto University Press, Kyoto)
- King, A.R., Davies, M.B., Ward, M.J., Fabbiano, G., & Elvis, M. 2001, ApJ552, L109
- Kubota, A., Tanaka, Y., Makishima, K., Ueda, Y., Dotani, T., Inoue, H., Yamaoka, K. 1998, PASJ, 50, 667
- Kubota, A. 2001, Ph.D. Thesis, University of Tokyo
- Lightman, A.P., & Eardley, D.M. 1974, ApJ, 187, L1
- Makishima, K et al. 2000, ApJ, 535, 632
- Matsumoto, R., Kato, S., Fukue, J., Okazaki, A. 1984, PASJ, 36, 71
- Mineshige, S., Hirano, A., Kitamoto, S., Yamada, T.T., Fukue, J. 1994, ApJ, 426, 308
- Mineshige, S., Wheeler, J.C. 1989, ApJ, 343, 241
- Mineshige, S., Kawaguchi, T., Takeuchi, M., & Hayashida, K. 2000, PASJ, 52, 499
- Mineshige, S., Osaki, Y. 1985, PASJ, 37, 1

- Mirabel, I.F., Dhawan, V., Chaty, S., Rodriguez, L.F., Marti, J., Robinson, C.R., Swank, J., & Geballe, T.R. 1998, *ApJ*, 330, L9
- Mirabel, I.F., Rodriguez, L.F. 1994, *Nature*, 371, 46
- Mirabel, I.F., Rodriguez, L.F. 1999, *ARA&A*, 37, 409
- Mitsuda, K., Inoue, H., Koyama, K., Makishima, K., Matsuoka, M., Ogawara, Y., Shibazaki, M., Suzuki, K., Tanaka, Y., & Hirano, T. 1984, *PASJ*, 36, 741
- Mizuno, T., Kubota, A., & Makishima, K. 2001, *ApJ*, 554, 1282
- Naik, S., Agrawal, P.C., Rao, A.R., & Paul, B. 2002, *MNRAS*, 330, 487
- Ohsuga, K., Mineshige, S., Watarai, K. 2002, *ApJ*, submitted
- Paczynsky, B., Wiita, P.J. 1980, *A&A*, 88, 23
- Rao, A.R., Yadav, J.S., & Paul, B. 2000, *ApJ*, 544, 443
- Ross, R.R., Fabian, A.C., Mineshige, S. 1992, *MNRAS*, 258, 189
- Sakimoto, P. J., & Coroniti, F. V. 1981, *ApJ*, 247, 19
- Shakura, N.I., Sunyaev, R.A. 1973, *A&A*, 24, 337
- Shakura, N.I., Sunyaev, R.A. 1976, *MNRAS*, 175, 613
- Shimura, T., Takahara, F. 1995, *ApJ*, 445, 780
- Shimura, T., Manmoto, T. 2003, *MNRAS*, 338, 1013
- Shibazaki, T., Hōshi, R. 1975, *Prog. Theor. Phys.*, 54, 706
- Szuskiewicz, E., Malkan, M.A., Abramowicz, M.A. 1996, *ApJ*, 458, 474
- Szuskiewicz, E., Miller, J.C. 1997, *MNRAS*, 287, 165
- Szuskiewicz, E., Miller, J.C. 1998, *MNRAS*, 298, 888
- Szuskiewicz, E., Miller, J.C. 2001, *MNRAS*, 328, 36
- Takeuchi, M., Mineshige, S. 1998, *ApJ*, 505, L19
- Taam, R. E., Chen, X., & Swank, J. H. 1997, *ApJ*, 485, L83
- Tanaka, Y., Lewin, W. H. G. 1995, in *X-ray Binaries*, ed W. H. G. Lewin, J. van Paradijs, W. P. J. van den Heuvel (Cambridge University Press, Cambridge) p126
- Wang, J.M., Zhou Y.Y., 1999, *ApJ*, 516, 420
- Watarai, K., Fukue, J. 1999, *PASJ*, 51, 725
- Watarai, K., Fukue, J., Takeuchi, M., Mineshige, S. 2000, *PASJ*, 52, 133
- Watarai, K., Mizuno, T., Mineshige, S. 2001, *ApJ*, 549, L77 (WMM01)
- Watarai, K., Mineshige, S. 2001, *PASJ*, 53, 915
- Yamaoka, K., Ueda, Y., Inoue, H. 2001, *New Century of X-ray Astronomy*, ed H. Inoue., H. Kunieda.(ASP Conference Series Volume 251), 426
- Zampieri, L., Turolla, R., Szuskiewicz, E. 2001, *MNRAS*, 325, 1266